Atmos. Chem. Phys., 14, 9883–9901, 2014
www.atmos-chem-phys.net/14/9883/2014/
doi:10.5194/acp-14-9883-2014
© Author(s) 2014. CC Attribution 3.0 License.

Atmospheric Chemistry and Physics
Open Access

Drivers of column-average CO_2 variability at Southern Hemispheric Total Carbon Column Observing Network sites

N. M. Deutscher[1,2], V. Sherlock[3,], S. E. Mikaloff Fletcher[3], D. W. T. Griffith[1], J. Notholt[2], R. Macatangay[1,*], B. J. Connor[4], J. Robinson[5], H. Shiona[5], V. A. Velazco[1], Y. Wang[2], P. O. Wennberg[6], and D. Wunch[6]**

[1]Centre for Atmospheric Chemistry, University of Wollongong, Wollongong, NSW, 2522, Australia
[2]Institute of Environmental Physics, University of Bremen, 28334, Bremen, Germany
[3]National Institute of Water and Atmospheric Research, Wellington, New Zealand
[4]BC Consulting, Alexandra, New Zealand
[5]National Institute of Water and Atmospheric Research, Lauder, New Zealand
[6]California Institute of Technology, Pasadena, CA, USA
[*]now at: Institute of Environmental Science and Meteorology, University of the Philippines, Diliman, Quezon City, Philippines
[**]now at: Laboratoire des Sciences du Climat et l'Environnement, CEA-CNRS-UVSQ, IPSL, Gif sur Yvette, France

Correspondence to: N. M. Deutscher (n_deutscher@iup.physik.uni-bremen.de)

Received: 10 April 2013 – Published in Atmos. Chem. Phys. Discuss.: 3 June 2013
Revised: 22 July 2014 – Accepted: 13 August 2014 – Published: 18 September 2014

Abstract. We investigate factors that drive the variability in total column CO_2 at the Total Carbon Column Observing Network sites in the Southern Hemisphere using fluxes tagged by process and by source region from the CarbonTracker analysed product as well as the Simple Biosphere model. We show that the terrestrial biosphere is the largest driver of variability in the Southern Hemisphere column CO_2. However, it does not dominate in the same fashion as in the Northern Hemisphere. Local- and hemispheric-scale biomass burning can also play an important role, particularly at the tropical site, Darwin. The magnitude of seasonal variability in the column-average dry-air mole fraction of CO_2, X_{CO_2}, is also much smaller in the Southern Hemisphere and comparable in magnitude to the annual increase. Comparison of measurements to the model simulations highlights that there is some discrepancy between the two time series, especially in the early part of the Darwin data record. We show that this mismatch is most likely due to erroneously estimated local fluxes in the Australian tropical region, which are associated with enhanced photosynthesis caused by early rainfall during the tropical monsoon season.

1 Introduction

Anthropogenic emissions of carbon dioxide (CO_2) are the most important driver of human-induced climate change. Understanding the temporal and spatial variability of sources and sinks of CO_2 is critical to modelling the processes that will contribute to future changes in atmospheric CO_2, anthropogenic radiative forcing and resulting climate impacts reliably. One widely used method is derived from atmospheric inverse modelling, in which estimates to the atmosphere are optimized using measurements of CO_2 (Enting and Mansbridge, 1989; Tans et al., 1990). These estimates are constrained by a relatively dense observing network on the global scale and in some regions (Peylin et al., 2013). However, several regions of importance to the carbon cycle, e.g. Siberia, South America and Africa, are poorly constrained because of a lack of measurements in those locations, as illustrated by the network of in situ sites shown in Fig. 1. In comparison to Western Europe and North America, there are also few measurements in Australasia. Altogether, this means that surface CO_2 fluxes in the Southern Hemisphere are particularly poorly constrained by in situ surface measurements.

The inference of surface fluxes from in situ measurements requires accurate modelling of atmospheric tracer transport, in particular, vertical mixing in the boundary layer and transport to the free troposphere. Errors in modelled transport are aliased into surface flux estimates. For example, Stephens et al. (2007) show that the spatial partitioning of a posteriori fluxes from inversions using a suite of transport models (but otherwise identical setups) was highly dependent on the strength of model vertical mixing.

Vertically integrated CO_2 column concentrations are less sensitive to vertical redistribution of the tracer than in situ measurements. Thus column abundance measurements are expected to provide complementary information to surface in situ measurements when included in surface flux inversions. Column measurements can also potentially provide information on remote locations, because they are influenced by a larger spatial area than surface in situ measurements (Keppel-Aleks et al., 2011). This comes at the expense of potentially more-detailed information about local fluxes. Quasi-global coverage of column measurements of CO_2 will be achieved via satellite platforms, such as SCIAMACHY (Burrows et al., 1995), GOSAT (Kuze et al., 2009), OCO-2 (Crisp et al., 2004) and CarbonSat (Bovensmann et al., 2010). Southern Hemisphere data from the Total Carbon Column Observing Network (TCCON) play an important role in satellite validation (e.g. Butz et al., 2011; Crisp et al., 2012; Morino et al., 2011; Reuter et al., 2011), and the low observed variability in the extratropical Southern Hemisphere has been exploited to derive a bias correction for ACOS GOSAT X_{CO_2} retrievals (Wunch et al., 2011b).

Previous studies investigating X_{CO_2} in conjunction with models (e.g. Yang et al., 2007) have focused on the Northern Hemisphere. Keppel-Aleks et al. (2011) show that column measurements are influenced by hemispheric scale flux patterns, and that synoptic variability in extratropical Northern Hemisphere X_{CO_2} is primarily related to large-scale meridional gradients in fluxes from the terrestrial biosphere. In a subsequent study, Keppel-Aleks et al. (2012) used TCCON data to show that simulations based on unoptimised biospheric fluxes from a version of CASA underestimated the seasonal cycle magnitude in column CO_2 due to a 40% underestimate of the strength of boreal flux seasonal cycle and a mismatch in the timing of the boreal drawdown. Basu et al. (2011) show an underestimate of the modelled seasonal cycle magnitude with CarbonTracker when compared to northern hemispheric TCCON data, a robust finding with those flux estimates regardless of the transport model used.

Houweling et al. (2010) compared four transport models driven by the same fluxes and meteorological reanalyses to four TCCON sites, including Darwin, Australia as well as the Northern Hemisphere sites Park Falls, Spitsbergen and Bremen. The comparison highlighted that the agreement in seasonal cycle shape was reasonable for the Northern Hemisphere sites. However, there was an obvious failure to reproduce the shape of seasonal cycle at Darwin in 2006 in any of the models. This suggests that there is a systematic failing in either the underlying fluxes or the transport driving these models. The models used by Houweling et al. (2010) included TM5, the model that underlies the CarbonTracker data assimilation study, and TM3, which is also used in our study.

In this study, we investigate driving factors behind variability in Southern Hemisphere X_{CO_2} measurements taken within the TCCON. Whereas previously the Southern Hemisphere has attracted relatively little interest because of the smaller, relatively quiescent landmass, a recent study suggests that the Southern Hemisphere, and in particular Australia, is responsible for almost 60 % of carbon uptake during interannual anomalies (Poulter et al., 2014). This interannual variability in uptake by Australian ecosystems in linked to precipitation changes. We examine the variability at the Southern Hemisphere TCCON sites via comparison of the measurements with simulations from the CarbonTracker data assimilation system (Peters et al., 2007) and a separate tagged tracer model run, both driven by the same best-estimate fluxes of CO_2 to and from the atmosphere. An alternative terrestrial biosphere tracer based on the Simple Biosphere model (Baker et al., 2003; Denning et al., 1996; Sellers et al., 1986) is also analysed. We investigate the processes and regions that are responsible for the simulated and measured variations in X_{CO_2}. In addition, we examine the causes of disagreement between measured and modelled time series of X_{CO_2}, in particular the seasonal mismatch in 2006 described in Houweling et al. (2010).

The paper is laid out as follows: Sect. 2 describes the models used and Sect. 3 the measurements to which they are compared. In Sect. 4 we investigate the variability in modelled X_{CO_2} while in Sect. 5 we compare the simulations to TCCON measurements, and investigate causes of discrepancies. The conclusions follow in Sect. 6.

2 Atmospheric transport modelling

2.1 CarbonTracker 2011_oi

The primary tool we use to investigate drivers of variability in the measured X_{CO_2} time series is the CarbonTracker (Peters et al., 2007) 2011_oi (hereafter "CT2011_oi") data assimilation product, available at http://carbontracker.noaa.gov. Model CO_2 is provided on 25 or 34 vertical levels (before and after December 31, 2005, respectively) for each TCCON site. The model is run with 3° longitude × 2° latitude global resolution, with 1° × 1° "zoom" over North America. CT2011_oi provides estimates of CO_2 fluxes to (or from) the atmosphere from biomass burning, fossil fuel emissions, the terrestrial biosphere and oceans. Details of the source of prior estimates of these fluxes are given in Table 1. In CT2011_oi an ensemble of prior fluxes is used, with two different estimates for each of the fossil fuel, biosphere and ocean components. The

Table 1. Details of CT2011_oi prior and posterior fluxes used in this comparison.

Flux	Source of prior flux	Optimized (Yes/No)
Biomass burning (BB)	GFED-CASAv3	No
Fossil fuel (FF)	CDIAC extended to 2009–2010 via 2011 BP energy consumption statistics	No
	ODIAC (Oda and Maksyutov, 2011) extended to 2008–2010 via 2011 BP energy consumption statistics	No
Ocean (OC)	Jacobson et al. (2007)	Yes
Terrestrial biosphere (TB)	GFED-CASAv2	Yes
	GFED-CASAv3	Yes

data assimilation system optimizes the terrestrial biosphere (TB) and oceanic flux (OC) components, while the fossil fuel and biomass burning components fluxes are unchanged from their prior values, described in Table 1. In the vertically resolved simulations at the TCCON sites, CO_2 total, background and process-specific mole fractions are provided every 1.5 h from 1 January 2000 to 31 December 2010. CarbonTracker uses the TM5 atmospheric transport model (Krol et al., 2005).

2.2 The Simple Biosphere model

In addition to the CarbonTracker optimized fluxes, we also use the monthly mean net ecosystem exchange (NEE) fluxes from the Simple Biosphere (SiB) model (Baker et al., 2003; Denning et al., 1996; Sellers et al., 1986) as an alternative terrestrial biosphere component. Messerschmidt et al. (2013) showed that the amplitude and phasing in SiB better matches that measured at Northern Hemisphere TCCON sites than either CASA or GBiome-BGC. This is used to assess how robust the regional and process attributions are to errors in the terrestrial biosphere fluxes, which could be an issue especially in data-sparse regions where posterior flux estimates are largely determined by the prior estimates (GFED-CASA in CT2011_oi). SiB has a balanced biosphere, meaning that the average annual net uptake is not captured and no long-term trend results from the terrestrial biosphere tracer.

2.3 Tagged tracer modelling with TM3

In addition to CT2011_oi, which provides model tracers separated by source process, we perform an additional tagged tracer model simulation to investigate regional influences. For this we use Tracer Model 3 (TM3) (Heimann and Körner, 2003) as the atmospheric transport model. The fluxes are run independently through the model, separated out into different tracers by process – biomass burning (BB), fossil fuel (FF), ocean (OC) and the terrestrial biosphere (TB) – for both CT2011_oi and SiB and by region. The regions used are largely based on the TransCom 3 regions (Gurney et al., 2002) – however, "Australia" is divided into four regions: tropical (north of 23° S) and temperate Australia, and the north and south islands of New Zealand. The regions are shown in Fig. 1. This results in a total of 14 land regions and 11 ocean regions, and a global total of 67 tracers.

TM3 is an offline model that is driven by reanalysis winds. In this case, we used winds from the NCEP reanalysis project (Kalnay et al., 1996). We used the fine-grid version of the model, which has a horizontal resolution of approximately 3.8° by 5° and 19 vertical levels. TM3 has been included in a wide range of model intercomparison studies (e.g. Gurney et al., 2002; Stephens et al., 2007). Stephens et al. (2007) found that TM3 was amongst the best three of the TransCom models at reproducing vertical gradients observed by aircraft profiles, though no model reproduced the vertical gradients in the measurements at all times. Furthermore, this model has been shown to be in excellent agreement with three other models in its representation of column CO_2 at four TCCON sites, including Darwin (Houweling et al., 2010).

The model is run from 2000 to 2010 inclusively. With no TCCON FTIR measurements before 2004, we are able to treat the years 2000–2003 as a spin-up period, allowing time for vertical and horizontal gradients to be well established, and therefore exclude model output that pre-dates the measurement time series. Unlike for CT2011_oi, we sample the TM3 model once a day, at 00:00 UT, at the locations of the TCCON sites. Temporal sampling biases were checked using the full temporal resolution CT2011_oi time series sampled at measurement times and at 00:00 UT, and the differences in the monthly means were found to be less than 0.1 µmol mol^{-1}.

TM3 simulations have been checked here for agreement with the CT2011_oi products for each source component. Both the CT2011_oi and TM3 time series are linearly detrended using the same linear factors, and agree to within 0.1 µmol mol^{-1} on monthly timescales, not only for the total CO_2 but also for each individual process. This agreement is consistent with the previous work of Houweling et al. (2010), who compared simulations of X_{CO_2} at four TCCON stations from a wider range of models and found remarkably similar results across all of the models used, which included both

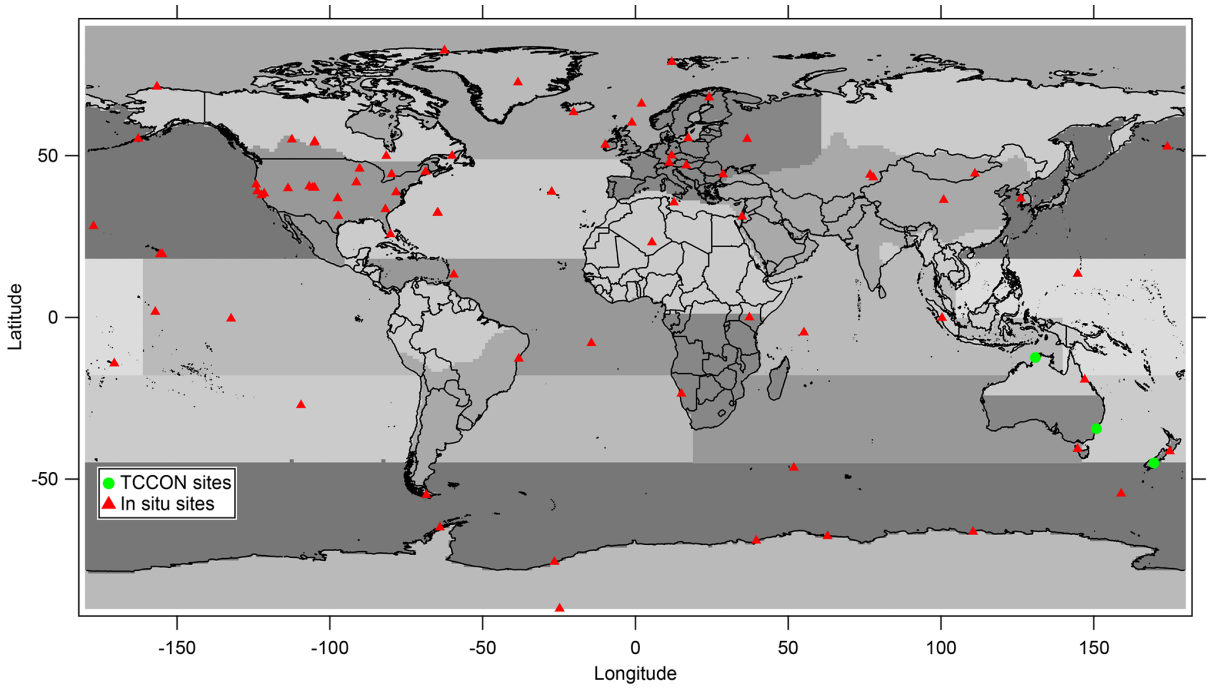

Figure 1. A world map showing the TCCON sites used in this study (green circles), other in situ sampling sites (red triangles) and the model aggregation regions used in this study, which are based on the TransCom regions.

TM3 and TM5. This gives us confidence in using our detrended model runs decomposed into the component regional tracers, although these simulations could still be sensitive to model biases that are common to all coarse-resolution global models. For comparison in terms of X_{CO_2}, the SiB terrestrial biosphere tracer is added to the fossil fuel, biomass burning and oceanic output from CT2011_oi, and then detrended.

2.4 GEOS-Chem

To provide model simulations from a model outside the TM family, we include simulations using the CT2011_oi optimized fluxes run via the GEOS-Chem model (Bey et al., 2001). The simulations are conducted using GEOS5 meteorology from 2004 to 2010 inclusively. Each process is modelled as a separate tracer on a 2° by 2.5° degree horizontal grid with 47 vertical levels with hourly output. We do not extensively use the GEOS-Chem simulations, as they are extremely similar to the simulations using the TM3 and TM5 models with identical fluxes, except in Sect. 4.2 and to comment on small but significant differences.

3 Measurement sites

We use measurements and simulations at the three existing Southern Hemisphere TCCON sites in Australia and New Zealand: Darwin, Wollongong and Lauder. The details for these sites are given in Table 2 and they are shown on the map in Fig. 1. Calibration of these sites occurred during the Tropical Warm Pool International Cloud Experiment (TWP-ICE) (Darwin) (Deutscher et al., 2010) and HIaper Pole-to-Pole Observations (HIPPO) (Wofsy et al., 2011) campaigns, and agrees well with the remainder of TCCON (Wunch et al., 2010).

The sites are situated in quite different environments. Darwin, until the recent establishment of the sites at Ascension Island and Reunion Island, was the only tropical TCCON site. Wollongong and Lauder are both SH mid-latitude sites – however, Lauder is located inland, in a dry environment dominated by farming, while Wollongong is a coastal site close to well-populated areas and industry to the north, and native forest and less dense population to the south and west. Further details about the sites, their instrumentation, uncertainties related to the data and the smoothing of the model to account for measurement a priori and averaging kernels are given in Appendix A. As discussed in Appendix A2, we take a value of 0.4 µmol mol^{-1} to be the threshold for a flux signature to be detectable in the TCCON measurements.

In situ FTIR analysers (Griffith et al., 2012) have been operating at Lauder since January 2007, at Darwin since March 2007 and sporadically at Wollongong. However, exploring additional info on fluxes from remote, undersampled source regions using surface-column contrasts at SH TCCON sites also requires careful characterisation of in situ measurement errors. This is beyond the scope of this study and will be addressed in future work.

Table 2. Sites used in this study.

Site	Latitude (° S)	Longitude (° E)	Altitude (m a.s.l.)	Instrument	Measurement years
Darwin	12.425	130.891	30	125HR	08/2005–present
Wollongong	34.406	150.879	30	125HR	05/2008–present
Lauder	45.038	169.684	370	120HR	2004–present
				125HR	2010–present

4 Modelled variability in X_{CO_2} at SH sites

Figure 2 shows the measured daily average time series, along with the CT2011_oi simulated time series, sampled at the measurement times and smoothed using the TCCON a priori and averaging kernels (see Appendix A3). It is apparent that there is a yearly increase of approximately 2 µmol mol^{-1} in the model simulated time series. Also obvious is that the intra-annual variability, or seasonal cycle, is relatively small, but not fully represented in CT2011_oi. To further investigate the magnitude of the seasonal cycles, we look now at the detrended time series for each site.

The time series are detrended by removing the average secular increase, calculated over an integer number of years, and then setting the mean of the time series to zero. The calculated trends are summarized in Table 3. We choose to use independent trends for each individual site and model time series, to encompass the different periods. The detrended time series are then used to investigate the magnitude of variability observed and expected at each site. For the model, we can examine both the total signature in X_{CO_2} and the components decomposed by process and source region. For the fossil fuel tracer, we also investigate detrending with a parabolic, rather than linear, function to account for the exponential increase in this tracer. Over the relatively short time series, the use of a parabolic fit instead of exponential causes differences of less than 0.05 µmol mol^{-1}. Neglecting the curvature, however, introduces approximately 2 µmol mol^{-1} difference to the detrended time series and significantly impacts the variability inferred in the mean seasonal cycles (MSCs). To maintain the equality between the sum of the tracers and the total X_{CO_2} we detrend all tracers with a linear function, but assess the interannual variability in the fossil fuel tracer relative to a parabolic function.

Figure 3 shows the derived MSCs. These are calculated from the monthly mean of the detrended and normalized time series, averaged for each individual calendar month over multiple years. The error bars give an indication of the magnitude of the interannual variability, as determined from the standard error for each month. From top to bottom (north to south), we can see that the magnitude of the seasonal variability in modelled X_{CO_2} gets smaller, and in all cases the amplitude is smaller than that of the yearly increase, at 0.8–1.5 µmol mol^{-1}. The magnitude of seasonal variability is quite small in comparison to the Northern Hemisphere TCCON sites such as Park Falls, Białystok and Orléans, which have a measured seasonal cycle magnitude of around 10 µmol mol^{-1} (Keppel-Aleks et al., 2011). The cycle magnitude is, however, larger than our 0.4 µmol mol^{-1} detectability criterion. Regarding the shape of the seasonal cycle, Lauder and Wollongong follow something resembling a sinusoidal pattern, with distinct (as much as can be with a small amplitude) yearly maxima and minima, and period of one year. Darwin shows more peculiar behaviour, with two distinct maxima and minima each year, and the early 2006 minimum as seen in Fig. 2 in particular means that there is a large apparent measurement–model difference in DJF.

Table 3. Comparison of yearly trends between FTS measurements and CT2011_oi smoothed column X_{CO_2}. All values are given in µmol mol^{-1} yr^{-1} ± standard deviation.

Site	FTS trend	CT2011_oi trend	Global surface trend
Darwin	2.17 ± 0.08	1.93 ± 0.05	1.96
	1.85 ± 0.10	1.98 ± 0.07	from monthly
	2.01 ± 0.07	1.92 ± 0.06	differences excluding January–June 2006
Wollongong	1.75 ± 0.16	1.79 ± 0.11	2.02*
Lauder	1.84 ± 0.04	1.86 ± 0.04	1.96

* Calculated from the integer years 2009 and 2010.

Figure 4 shows the modelled simulated MSCs for each site for CT2011_oi, both for the total CO_2 and decomposed by source process. Data shown here are based on all model values for 2003–2010 inclusively. Also included are the total CO_2 and terrestrial biosphere tracers using SiB. The MSCs are seasonal anomalies with respect to a secular trend, and the sign of the anomalies therefore does not necessarily reflect the sign of the fluxes themselves. The lines in the lower (main) section of each plot show the MSC in X_{CO_2} while the upper panel gives the standard error in the MSC – an indication of the interannual variability (IAV) in each component.

At all three sites, the simulated contribution of the fossil fuel and ocean fluxes to variability is small, and the terrestrial biosphere signal dominates the seasonality. For Darwin, there is a significant signal due to biomass burning;

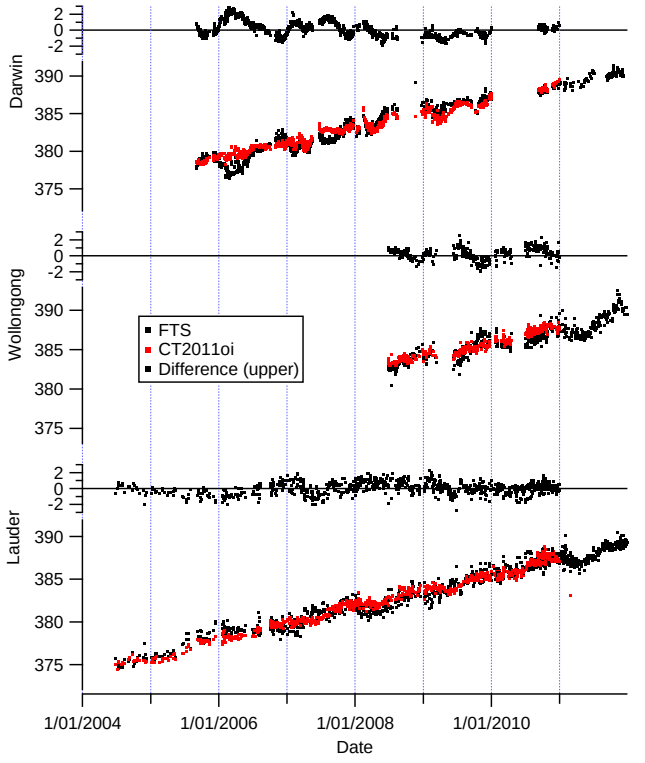

Figure 2. Measured (black) and CT2011_oi modelled (red) daily average time series of X_{CO_2} at the three Southern Hemisphere TCCON sites. For each site, the difference between the modelled and measured (measured–modelled) values is given in a separate panel. The model output are interpolated to the times of the FTS measurements, and then smoothed with the FTS a priori and averaging kernel profiles.

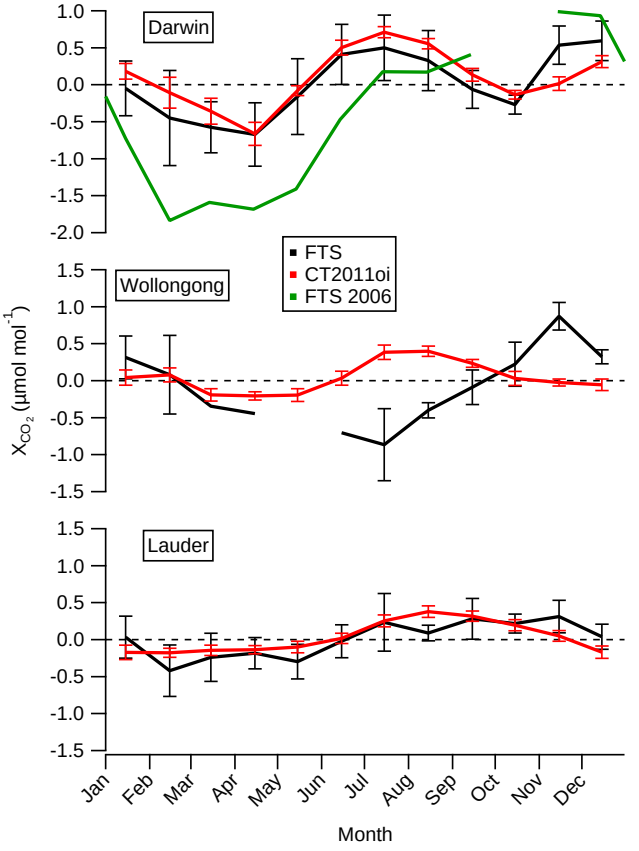

Figure 3. Derived mean seasonal cycles for the FTS (black) and CT2011_oi (red) time series for each site. The error bars are derived from the standard deviation of the mean difference within each month from a secular trend, and give an indication of the interannual variability. For Darwin, the MSC is derived from 2006 to 2010 inclusively, for Lauder 2005–2010 and Wollongong from only 2009–2010. For Darwin, a green trace is added to depict the measured monthly averages for the year 2006. Data gaps exist due to incomplete measurement records, caused by a combination of poor measurement conditions and instrumental problems.

the magnitude of seasonality with a late year maximum is 0.5 µmol mol^{-1}, comparable with the limit of detectability. Compared to CT2011_oi, SiB exhibits a larger seasonal cycle amplitude at the extratropical sites, and behaves quite differently around the change of the calendar year in Darwin.

With respect to the IAV, the terrestrial biosphere is the largest contributor at each site. The fact that the terrestrial biosphere IAVs are generally larger than the IAV in the total X_{CO_2} implies that there is an anti-correlation between the terrestrial biosphere anomalies and those of another process or processes. The biomass burning, surprisingly, has the smallest IAV for each site, perhaps an indication that the prescribed BB fluxes do not capture the full IAV of biomass burning emissions and real variability in this flux is ascribed by the data assimilation system to the terrestrial biosphere flux. Mu et al. (2011) indeed showed that including higher frequency variability in fire emissions improved model simulations. The oceanic flux also has a small IAV. In contrast, a previous analysis of the processes contributing to variability in surface CO_2 (Nevison et al., 2008) shows that in the Southern Hemisphere this is dominated by the terrestrial biosphere but also has a significant contribution to IAV from oceanic fluxes. The total column therefore potentially is exposed to different signals than the existing baseline surface network dominating that analysis. Some additional qualitative analysis and discussion of the surface variability at the TCCON sites is given in the Supplement.

In terms of the seasonal patterns, the bi-modal seasonality previously noted at Darwin is driven by the terrestrial biosphere and dynamics, while the other sites show more sinusoidal behaviour, with maximum X_{CO_2} in mid-to-late Southern Hemisphere winter, also driven by the terrestrial biosphere. The other flux components serve to slightly dampen the terrestrial biosphere signal, and therefore the seasonal cycle. To investigate which region is the source of the double seasonality at Darwin, we look at the TM3 model run with the source processes further decomposed by region.

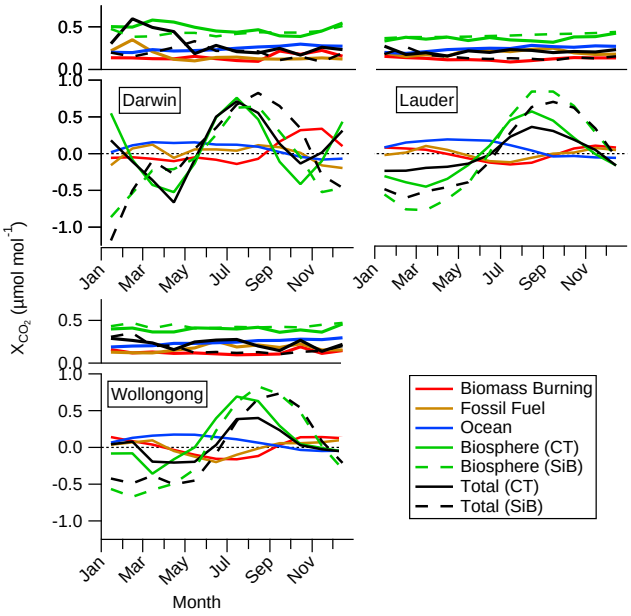

Figure 4. Mean seasonal cycles (bottom panels) and interannual variability (top panels) in the CT2011_oi simulation for the Southern Hemisphere TCCON sites Darwin (top left), Wollongong (bottom) and Lauder (top right), decomposed by source process: total (black), biomass burning (red), ocean (blue), terrestrial biosphere (green) and fossil fuel (brown). The MSC for the SiB terrestrial biosphere is also shown in dashed green. For each site the magnitude of the interannual variability is derived from the standard deviation in the derived MSC.

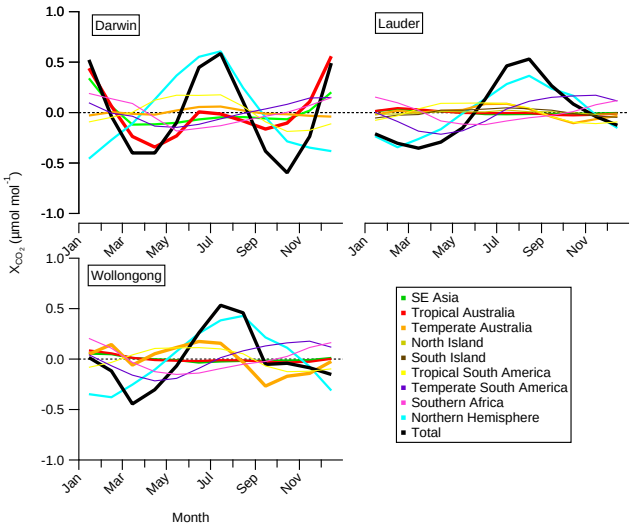

Figure 5. Regional decomposition of the mean seasonal cycles of the terrestrial biosphere in the TM3 simulation with CT2011_oi fluxes.

4.1 Regional decompositions

Attribution of CO_2 fluxes on regional scales via inverse model systems still results in large discrepancies between models (Peylin et al., 2013). This is especially true in regions with few atmospheric measurements, such as the Tropics and Southern Hemisphere (Peylin et al., 2013). Therefore, the following interpretations must be treated with caution. However, from the models used in the RECCAP ensemble (Peylin et al., 2013), CarbonTracker sits close to the mean, and can therefore be considered somehow representative of our current state of knowledge of regional-scale CO_2 flux estimates derived from atmospheric CO_2 inversions. Here we explore sensitivities to regional fluxes based on the current knowledge, in the attempt to better understand these processes.

4.1.1 Terrestrial biosphere

Figure 5 shows the decomposition of the terrestrial biosphere flux signal by region. We combine all Northern Hemisphere regions except Southeast Asia and combine South America and South Africa. In both cases, the shape of the MSCs from the composite regions is similar, and the aggregation serves therefore to show the net effect more clearly. For each site, the effect of the Northern Hemisphere can be clearly seen. A time lag exists between the fingerprint of the Northern Hemispheric biosphere at Darwin and those further south. The advection of the NH X_{CO_2} minimum is delayed at Darwin by approximately 4 months compared to the NH itself, and around 6 months at the extratropical sites. The bimodal seasonality seen at Darwin is a combination of the transport of the Northern Hemisphere flux minimum with the minimum produced from the biosphere in tropical Australia. The magnitude of the seasonality in the tropical Australian tracer is similar to that from the Northern Hemisphere, though with a less regular pattern, including a mid-year peak overlaid on a cycle that otherwise has a maximum in the Australian summer (tropical Australian wet season). In Wollongong, the significant contributors apart from the Northern Hemisphere flux are the temperate Australian region, as well as the combined South American and South African region. The South American and South African region also imparts a noticeable signal at Lauder. These model simulations indicate that under-sampled regions impart observable signatures in the SH TCCON measurements. However, unless the error in the estimated fluxes is of the same magnitude as the flux itself, these data will struggle to provide further constraints on fluxes from these remote regions until all potential measurement biases are eliminated.

The regional decomposition of the SiB terrestrial biosphere fluxes is shown in Fig. 6. The larger seasonal cycle amplitude in the SiB simulations compared to CT2011_oi is due to the differences in form and phasing of modelled fluxes from a number of regions. The Northern Hemispheric signal shows a broader peak with a less drastic drop-off than in the CT2011_oi simulation. At Darwin, the contribution from the tropical Australian signal is quite different between the two models, leading to the late-year X_{CO_2} minima and absence of

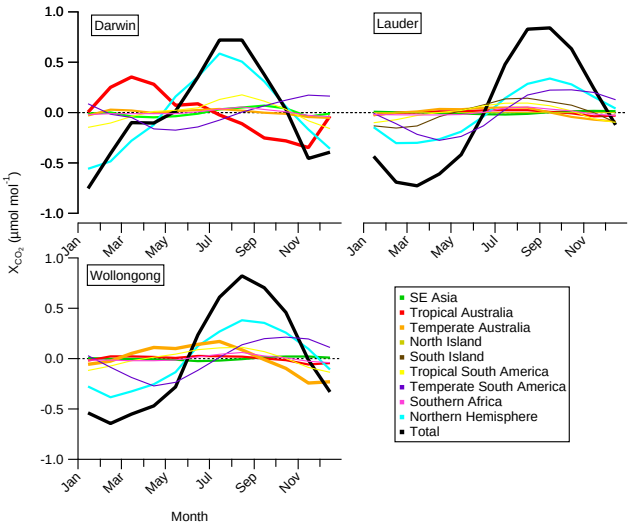

Figure 6. Regional decomposition of the mean seasonal cycles of the terrestrial biosphere in the TM3 simulation with SiB fluxes.

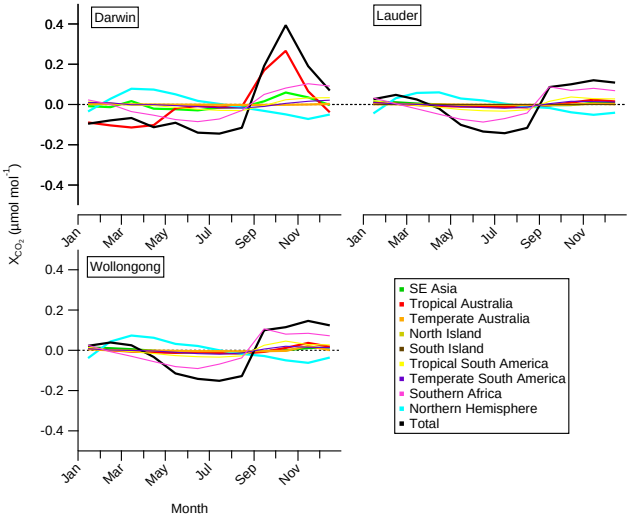

Figure 7. Regional decomposition of the mean seasonal cycles of biomass burning in the TM3 simulation with CT2011_oi fluxes.

the double-peaked seasonal cycle in the simulations with SiB fluxes. The contribution from the SE Asian region also shows considerably less seasonal variation in SiB than in the optimized CT2011_oi. At Lauder and Wollongong the seasonal cycle is primarily amplified by constructive superposition of contributions from the Northern Hemisphere (with delay due to transport) and the temperate Southern Hemisphere landmasses, including an amplified contribution from the South Island of New Zealand in the case of Lauder.

4.1.2 Biomass burning

Figure 7 similarly shows the breakdown by region for the unoptimised biomass burning fluxes, however with a smaller vertical axis range. The magnitude of seasonality is smaller than the detectability limit in all cases, though at all sites there is evidence of a signal from the combined South American and South Africa region, with magnitude close to this detectability limit. Jones et al. (2001) have previously presented evidence of annual long-range transport of biomass burning emissions being observed at Lauder. For Darwin, a local source from tropical Australia with an October peak is also apparent. Biomass burning has a large amount of interannual variability, so in addition to looking at the MSCs, in Fig. 8 we look at the detrended time series for a few of the tracers – the South America and South Africa region for each site, and the tropical Australian and Southeast Asia tracer at Darwin. The manifestation of the South America and South Africa tracer is very similar at all sites. Two years, 2007 and 2010, have seasonal cycle amplitudes that are of a magnitude that could allow them to be detected. At Darwin, the tropical Australian fire emissions show some interannual variability, with large peaks in late 2003, 2004, 2007 and 2009 and smaller peaks in other years. The Southeast Asian flux is generally small, except for late 2006 when large fires occurred in Indonesia (Nara et al., 2011; Paton-Walsh et al., 2010). This, and the peak years in the local fires, are of a magnitude that also could possibly be detected in the monthly mean TCCON X_{CO_2} values.

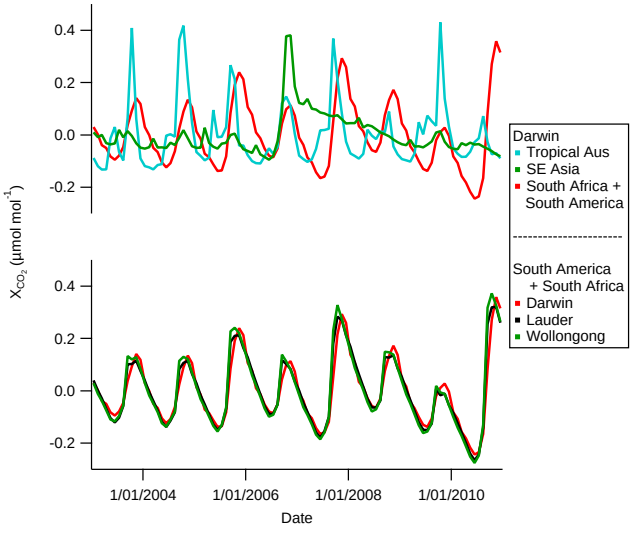

Figure 8. Time series of regional decomposition of the detrended time series for the South American and South African biomass burning tracer at all three sites and the tropical Australian and Southeast Asian tracers as sampled at Darwin.

The biomass burning fluxes are prescribed in the CT2011_oi data assimilation system based on GFEDv3 (van der Werf et al., 2010). Any errors in the prescribed biomass burning emission estimates are therefore likely to be attributed to co-located terrestrial biosphere fluxes during the flux optimisation process. We therefore investigate how well

biomass burning events are observed in the measurements. Here, we consider Australia and New Zealand to be local signals for all sites, while South America, Southern Africa and the Northern Hemisphere make up the remote component. SE Asia is considered local to Darwin but not to the other two sites. Figure 9 shows the linearly detrended time series of X_{CO} measured by the instrument at Darwin, along with the modelled biomass burning contribution to X_{CO_2} from a combination of Australian and Southeast Asian fires. We use the measured X_{CO} for validation of the modelled biomass burning fluxes, because CO is a good biomass burning tracer. In general, the timing of the features in both time series agrees well. Mu et al. (2011) previously used X_{CO} from Darwin and other sites to show that adding higher frequency variability to GFED fire emissions improved the performance of model simulations. There are regular signatures each year through September and October (and occasionally later) except in 2008 when there are missing data during the biomass burning season. The large peak in 2006 was due to large Indonesian fires that occurred that year (Paton-Walsh et al., 2010), while the other peaks all result from regular Australian savannah biomass burning. The background level in the modelled X_{CO_2} after the large 2006 fires stays enhanced relative to the measured X_{CO}, due to a persistent X_{CO_2} signal from those fires that is evident significantly longer than the atmospheric half-life of CO (∼2 months).

Using the detrended measurements, an emission ratio (CO / CO_2) of 0.1 mol mol^{-1} is inferred. This falls within the range of previously calculated emission ratios, such as those from Andreae and Merlet (2001) and Zhang et al. (2000) (0.050–0.130 mol mol^{-1}) for tropical forests, but is lower than the 0.171 mol mol^{-1} calculated by Nara et al. (2011) for the 2006 Indonesian fires and higher than savannah burning from Andreae and Merlet (2001) and Hurst et al. (1994) of 0.06 ± 0.02 mol mol^{-1}. The emission ratios assumed in the Global Fire Emissions Database (GFEDv3) (van der Werf et al., 2010), the source of the biomass burning fluxes in these model runs, for Indonesia and Northern Australia agree with those of Andreae and Merlet (2001) for tropical fires and savannah and grassland burning, respectively. One would expect the CO / CO_2 ratio measured here to be biased low relative to the actual emission ratio, because of the relatively shorter atmospheric lifetime of CO. Outside this event, there are a few periods of enhanced measured X_{CO} not predicted in the model X_{CO_2}, especially in 2008. Based on the agreement in timing between the modelled biomass burning tracer and the measured column CO data, we conclude that the GFEDv3 biomass burning estimate from local- to regional-scale fire sources is unlikely to be a leading source of biases in simulations of the X_{CO_2} at the Southern Hemisphere TCCON sites. However, given the range of emission factors published, the magnitude is still uncertain.

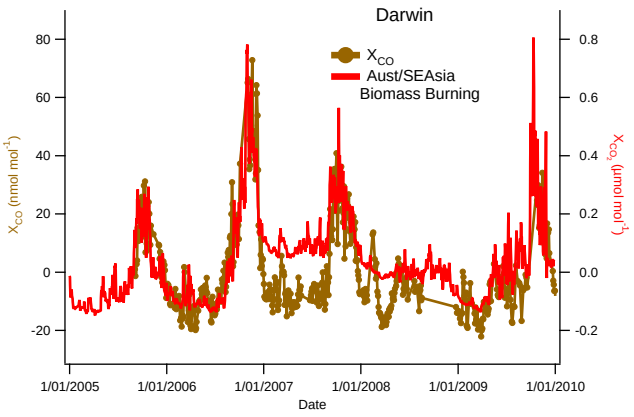

Figure 9. Linearly detrended time series of X_{CO} measured by the TCCON FTS at Darwin (brown) and the modelled contribution of local (Australian and Southeast Asian) biomass burning to the X_{CO_2} (red).

4.2 Dynamics

A multi-model assessment of transport and transport errors is beyond the scope of this study, but we attempt to give a quantitative assessment of the impact in interannual variability in the Southern Hemisphere X_{CO_2} time series by performing a model run using the analysed CT fluxes but using meteorology for a single year, 2001, for the entire time series. We then compare the X_{CO_2} time series simulated using the repeating and standard meteorology. Figure 10 shows the monthly mean time series of differences for each site. The largest differences are seen during the monsoon periods at Darwin, from January to March, with these periods indicated by the grey shading. It is at this time of the year that the Intertropical Convergence Zone (ITCZ) is furthest south. Circulation changes associated with El Niño–Southern Oscillation clearly play a role in transport-related interannual variability at Darwin. The upper panel in Fig. 10 shows the standard deviation calculated in deriving the MSC of the differences, giving an indication of the contribution of interannual variability in dynamics to the variability in X_{CO_2}. Outside of the period in January to March at Darwin, the differences caused by interannual variability in meteorology are smaller than 0.2 µmol mol^{-1}, and generally smaller than 0.1 µmol mol^{-1}. Despite the differences seen, the only instance where using fixed rather than varying meteorology impacts on the derivation of the MSC is in March at Darwin.

To additionally assess the impact of the transport models, and ensure that the use of models only from the TM family does not bias our results, we include GEOS-Chem simulations. Comparison between GEOS-Chem, TM5 and TM3 simulations using identical CT2011_oi fluxes for each of the processes shows that there are very minor differences for all three sites. Differences greater than 0.05 % X_{CO_2} occur sporadically and only in the fossil fuel tracer, indicating some

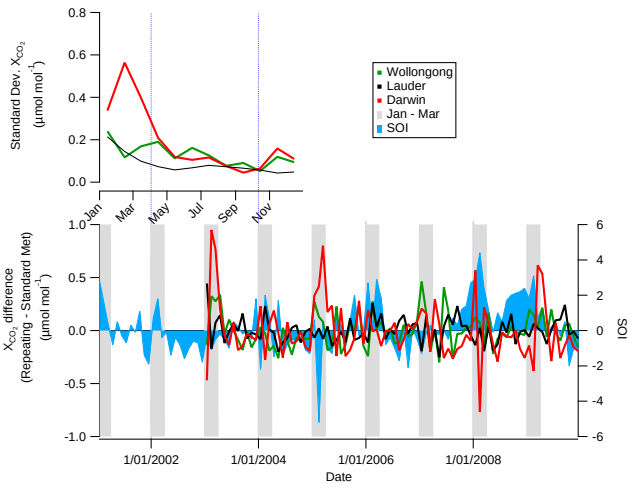

Figure 10. (Bottom) The monthly mean time series of differences between simulated X_{CO_2} with fixed 2001 or year specific meteorology, and (top) the standard deviation resulting from derivation of the MSC of these differences, representing the influence of interannual variability in dynamics on the interannual variability in X_{CO_2}. The Southern Oscillation Index (accessed from http://www.cpc.ncep.noaa.gov/data/indices/soi) is shown in blue.

potential differences in the timing of interhemispheric transport.

5 Evaluation of the simulations using TCCON

Having examined the simulated variability, and drivers thereof, in Southern Hemispheric column CO_2 amounts, we now compare the simulations to the measurement time series at the TCCON sites. The daily average X_{CO_2} time series are shown in Fig. 2. In general, the north-to-south latitudinal gradient between the sites is evident. Before detrending, we compare the measured and modelled trends at the sites and compare the measured and modelled time series.

The calculated trends are summarized in Table 3. To determine the trends for Wollongong and Lauder we take a simple linear fit to the monthly average measurements and model simulations. For Darwin, because of the relative irregularity of the seasonal cycle, and interannual variability in features such as the early year drawdown as seen in Fig. 2 in 2006, we investigate various means of calculating the trend in the time series. These are the aforementioned linear fit, a linear fit excluding the early 2006 values, and a calculation based on a simple difference between months in the first (2005) and last (2010) years common to the measurement and model time series. That is, we take the average yearly change between September through December 2005 and the corresponding months in 2010. In Table 3 we also present the global surface trend (Thomas Conway and Pieter Tans, NOAA/ESRL – www.esrl.noaa.gov/gmd/ccgg/trends/) over the time period of the FTS measurements. For Wollongong and Lauder the determined TCCON and CT2011_oi trends are in good agreement, certainly within the estimated uncertainties. For Darwin, the situation is more complex, but the best agreement comes from a linear fit to the data excluding early 2006. The determination based on differencing also agrees within uncertainties. The CT2011_oi trend is robust to all calculations, but the FTS-derived trend is more variable.

Figure 2 shows the comparison between the daily average measured and model time series, along with the difference (measurement–model mismatch) between them. The most striking feature is the failure of the model to capture the drawdown at Darwin in early (January–March) 2006 and to a lesser extent in early 2007. The 2006 mismatch is quite large, reaching 3 μmol mol^{-1}. There is also some apparent pattern to the mismatch at the other two Southern Hemisphere sites, though not as pronounced as that for Darwin.

To assess the robustness of the attributions to potential errors in the terrestrial biosphere fluxes we also include analysis based on the SiB terrestrial biosphere runs. Figure 11 shows the daily average linearly detrended time series from the TCCON measurements and both the CT2011_oi and SiB simulations. For Wollongong and Lauder, the SiB-based simulation seems to have a larger seasonal cycle amplitude than CT2011_oi. For Darwin, many variations are seen by both simulations; however, in general SiB produces a late-year minimum that precedes any minimum in CT2011_oi by some months.

We also return to the MSCs, shown in Fig. 3. Given that there are only two years of overlap, we cannot reliably interpret the Wollongong comparison. For Lauder, the differences between the modelled and measured MSCs are smaller than the detectability when averaging over multiple years. In Darwin the agreement is not quite so good, with the model underestimating the drawdown that occurs during December to February, resulting in underestimating X_{CO_2} in December, and overestimating it in January to March. This difference is of the order of the detectability limit, but is obviously strongly influenced by the years 2006 and 2007, where the difference is quite large. The error bars give an indication of the relative interannual variability between the model and measurements. The magnitude of the error bars indicates that at all sites the model predicts less interannual variability than measured. The error bars also indicate that in Darwin there is relatively little year-to-year variation during the middle of the year, from May to September, corresponding largely to the dry season. There is considerable IAV in the early months of the year, no doubt influenced by the large drawdown apparent in 2006. In Lauder the IAV is relatively consistent throughout the year; however, July and the early year exhibit larger variability. In each case, the measured IAV is greater than the detectability limit.

The comparison with SiB (Fig. 11) also fails to reproduce the early 2006 minimum at Darwin, as well as regularly underestimating the X_{CO_2} in the final months of the year. At Wollongong and Lauder, SiB tends to estimate an earlier

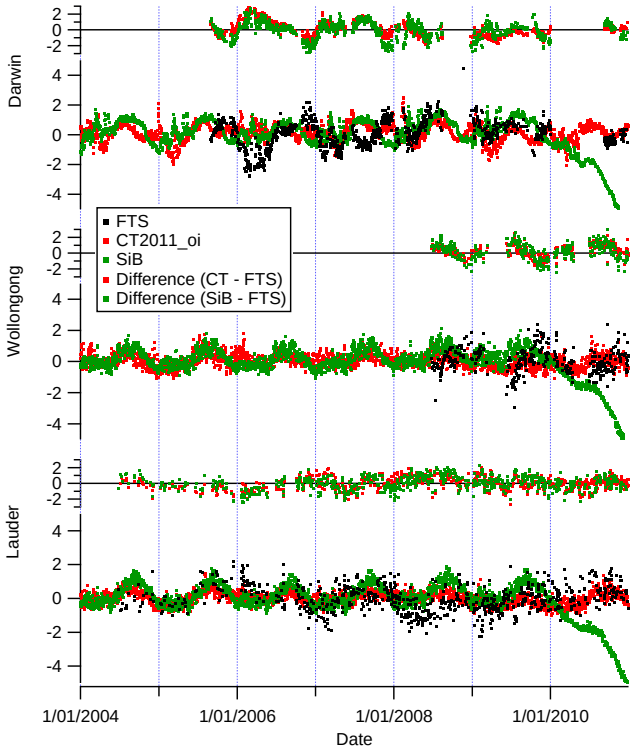

Figure 11. Linearly detrended daily average time series of TCCON (black), CT2011_oi (red) and SiB (green) at the SH TCCON sites, and the differences between the two models and the measurements (top panels).

maximum in the seasonal variation. A quantitative measure of the relative performance of CT2011_oi and SiB is given by the rms difference between the simulations and the daily average TCCON data (Table 4). For each site, the models more closely resemble each other than they do the measurements, but CT2011_oi provides a better match to the measurements than SiB. This is a reflection of the lack of data in the Southern Hemisphere available to optimize the fluxes, but that those data available do help to improve the fit to the measurements.

In evaluating the mismatches between the measurement and model time series, we refer to simulations of the dominant factors in the variability of X_{CO_2} at the Southern Hemisphere TCCON sites. Based on these, we expect that the mismatch must be driven by local or remote biosphere, transport, or biomass burning on the local to hemispheric scale. We now examine the terrestrial biosphere in detail.

5.1 Local biosphere

Given the relative lack of measurements in Australia and the Southern Hemisphere in general, there is little information to adjust SH fluxes in CarbonTracker if they are different from the a priori. It would therefore be unsurprising if there is a possible error in the estimate of the local biospheric flux,

Table 4. Root mean square (rms) calculated from the fit of the SiB and CT2011_oi based simulations to the daily average measured X_{CO_2}.

Site	CT2011_oi-FTS	SiB-FTS	SiB-CT2011_oi
Darwin	0.914	1.068	0.815
Wollongong	0.870	1.089	0.604
Lauder	0.798	0.875	0.524

hence we examine the possibility for this to cause the observed disagreement. To do this, we independently run a series of regionally tagged monthly pulse fluxes during the year of 2004, and examine their evolution in the model world at the TCCON sites. The pulses correspond to the optimized terrestrial biosphere fluxes for each region.

Figure 12 shows how the tropical Australian biosphere flux pulses are observed at all sites, normalized to their long-term effect on X_{CO_2}, that is, they settle to a normalized final value of 1. Each pulse produces a maximum X_{CO_2} change of about 1.5 µmol mol^{-1}, with a small long-term effect of less than 0.1 µmol mol^{-1}. A mis-estimation of such a flux would fit well with what is seen in the mismatch – a short-term disagreement that manifests itself in a net long-term effect that is close to zero. Given the lack of measurements available to constrain the fluxes in this region, and the small net signal, the net local flux could be biased in CT2011_oi by a large enough amount to account for the differences. We examine the effect of the tropical Australian biosphere at the other Southern Hemisphere sites to see if they can be detected in the measurements there. Figure 12 shows the pulse signals from the Australian tropical region at Wollongong and Lauder, with smaller *y* axis ranges. The signals seen here are also largest for February, but these still translate to X_{CO_2} values that are generally much smaller than the detectability limit. It is likely that such a signal, emitted from the Tropics in a highly convective region, is therefore only detectable in the short term on local spatial scales, especially as the magnitude relative to other fluxes is small. It can, however, have a large short-term signal and therefore could be responsible for model–measurement mismatches observed at Darwin.

We also examine the predicted and optimized fluxes for the tropical Australian region over the course of the measurement period. Figure 13 shows the optimized terrestrial biosphere fluxes from tropical Australia for each year from 2005 to 2010. The years 2006 and 2007 have the largest January fluxes, and in no year do the fluxes increment from the prior estimate by a considerable amount. These are therefore the years that the underlying biosphere model estimates to have the largest respiration-based fluxes to the atmosphere and also the years with the largest measurement–model mismatch. It is therefore very plausible that these could be overestimated fluxes, and as seen from the pulse runs, this could have a large short-term impact on the modelled columns.

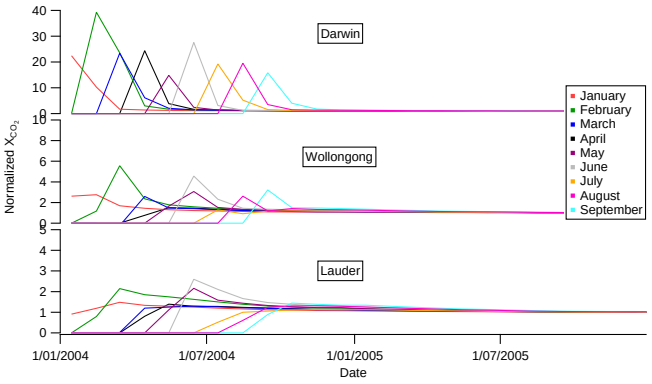

Figure 12. The time series of relative X_{CO_2} changes resulting from each month's terrestrial biosphere flux in the tropical Australian region. The X_{CO_2} values are normalized to the long-term value caused by the pulse in question and therefore are always positive, and indicate the relative ability of a flux from a particular month to affect the X_{CO_2}. The effect of each month's terrestrial biosphere flux reaches a maximum X_{CO_2} contribution of 1.5 µmol mol^{-1} at Darwin with a long-term effect of less than 0.1 µmol mol^{-1} at all sites.

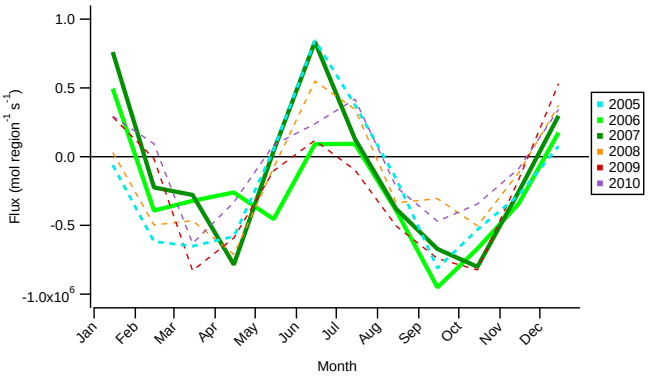

Figure 13. The optimized tropical Australian terrestrial biosphere fluxes for each year from 2005 to 2010.

The timing and magnitude of local biospheric fluxes are likely to be affected considerably by the timing of the monsoon onset. In the middle of the calendar year there is almost no rainfall, but still high temperatures. Plant photosynthesis, and hence CO_2 uptake, is known to be inhibited by water stress, and this is particularly sensitive at higher temperatures (Chaves et al., 2002). The sign of net ecosystem exchange could therefore change with the onset of the monsoon and consequent relief of water stress. Any interannual variability in the timing of the monsoon onset could therefore have an effect on the timing of the beginning of the growing season.

To examine this, we look at the rainfall measured at the Darwin ARM site, where the TCCON instrument is located. For each year from June 2005 to October 2009 we examine the cumulative rainfall between October 1 and March 31 the following year. This period is chosen to approximate the build-up and monsoon period. The cumulative rainfalls are shown in Fig. 14. June 2005 clearly stands out as having a much earlier significant rainfall, with more than 30 % on the total monsoonal rainfall having fallen during November 2005. This could lead to an earlier relief of water stress, and enhanced photosynthesis relative to other years, which contrasts with the prior biospheric fluxes estimated, and is a potential explanation for the mismatch between the model and the measurements seen in early 2006. Such a change in weather is accompanied by a change in dynamics, and as a result there could be an advective signal in addition to that from the local flux. Unfortunately, no in situ CO_2 measurements were available in Darwin in 2006.

Valsala et al. (2013) studied the intraseasonal variability of modelled biospheric CO_2 fluxes in India during summer monsoons. They found that in CarbonTracker (in this case with CT2010), positive rainfall anomalies correlate with positive flux anomalies, and hypothesise that this is due to the lack of photosynthetically active radiation occurring during rainfall periods, but that the onset of the rainy season initiates vegetation growth. As for northern Australia, the Indian subcontinent has few measurement data included in CarbonTracker (see Fig. 1) and therefore the posterior fluxes are poorly constrained and highly dependent on the priors. This positive correlation between rainfall and CO_2 fluxes seen in CarbonTracker is therefore probably driven by the GFED-CASA priors and may be an incorrect response at the time of monsoon onset. As seen from the number of solar absorption measurements obtained at Darwin in the 2005–2006 monsoon season, there were still numerous sunshine hours that would have facilitated photosynthetic activity.

Niwa et al. (2012) showed that inclusion of aircraft data into a CO_2 inversion significantly altered flux estimates over the Indian subcontinental region (their "South Asia") compared to inversions based on in situ data and priors based on similar priors to those used in CarbonTracker, including the use of CASA as the terrestrial biospheric prior. The net effect of the changed biosphere fluxes in this region is towards a larger-amplitude seasonal cycle, and an earlier uptake. While this change is subtle, it does suggest that CarbonTracker and CASA may not correctly capture the impact of monsoon onset on CO_2 biosphere fluxes.

The recent paper by Poulter et al. (2014), using a range of ecosystem models, suggests that there is a strong correlation between precipitation and annual carbon sink strength, which is particularly evident in Australia. This is supported by satellite-based vegetation products and upscaled flux measurements. This further suggests that CASA may not correctly model this short-term response.

We also now look at other possible drivers of this mismatch.

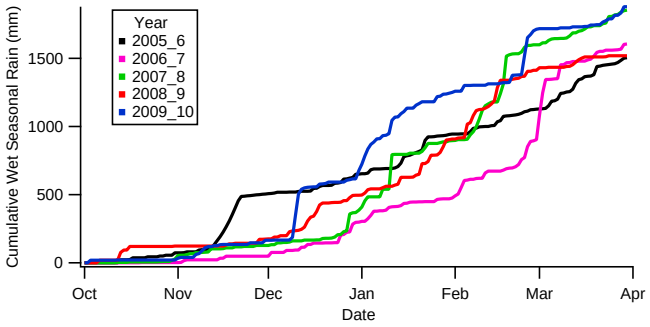

Figure 14. Cumulative rainfall through each monsoon season (October through to the following March) from June 2005 to October 2009 as measured at the ARM site.

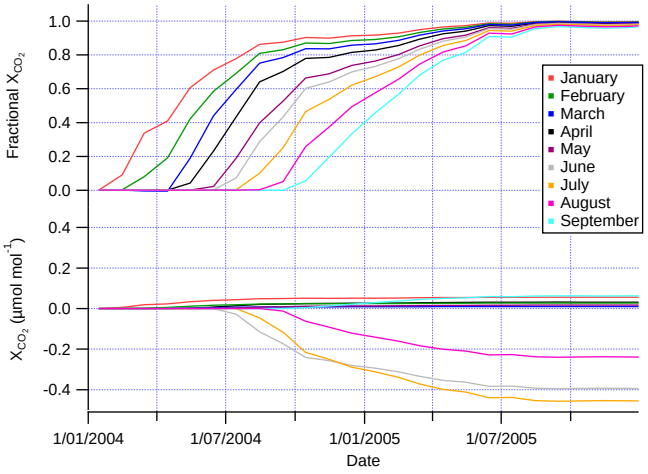

Figure 15. The cumulative fractional X_{CO_2} change at Darwin due to pulse fluxes for each month from the Northern Hemisphere boreal terrestrial biosphere (top) and the changes observed in X_{CO_2} due to the optimized flux for each month.

5.2 Influence of the Northern Hemisphere biosphere

We previously diagnosed the influence of transport using the TM3 simulation using fixed 2001 meteorology (Sect. 4.2). The greatest variability in transport from the Northern Hemisphere occurs for the tropical Darwin site. This variability occurs largely in the first months of the year, corresponding with the Indo-Australian monsoon season, and movement of the ITCZ, both in the month-to-month variations, and the interannual variability for each month. The modelled transport from the Northern Hemisphere is essentially constant from month-to-month and year-to-year at Wollongong and Lauder. The consistency at these sites means that any modelled variability in other NH tracers at these sites must be due to temporal variability in the corresponding fluxes.

Previous studies have suggested that the magnitude of the seasonal cycle of biospheric uptake in boreal regions is underestimated (Keppel-Aleks et al., 2012; Yang et al., 2007). We consider this, coupled with the delay due to meridional transport, to be a candidate for causing the model overestimation in early 2006 and 2007 at Darwin that is shown by the model–measurement comparisons in Figs. 2 and 3. To examine this possibility, Fig. 15 shows the manifestation of the 2004 NH boreal fluxes at Darwin. The maximum influence is considerably earlier than the timing of the mismatch between modelled and measured X_{CO_2}, suggesting that transport of the boreal uptake period is seen in the column CO_2 data relatively quickly, within three to four months as also shown by the timing of the minimum in the Northern Hemisphere terrestrial biosphere tracer at Darwin. The SF_6 TransCom study (Denning et al., 1999) suggested that full 3-D (i.e. column) atmospheric exchange occurs about twice as fast as it manifests at the surface for TM3, and also found that TM3 had a comparatively slow interhemispheric exchange time but good agreement simulating SF_6 distributions. Peters et al. (2004) also show that TM3 and TM5 have relatively slow interhemispheric transport, influenced by slow vertical transport within the models. However, the differences in the fossil fuel tracers between the TM models and GEOS-Chem, which can be attributed to interhemispheric transport differences, do not occur at the time of the model–measurement mismatch, so the mismatch is not specific to the TM models and their slow interhemispheric exchange. In addition, the total influence of the Northern Hemisphere is only on the order of 1 µmol mol^{-1}, so even if the strength of the uptake were to be underestimated by 40%, which is not true for the CT2011_oi optimized fluxes, then the manifestation at Darwin would not result in such a large mismatch. A large underestimation of the flux would also result in a large net effect to the CO_2 time series (0.5 µmol mol^{-1} or greater) that would need to be negated by balancing in another region or via contrasting flux at another time period. The apparent slow interhemispheric transport of TM3 and TM5 is therefore not the main driver of the mismatch seen at Darwin, but may still play a role in model–measurement disagreements in the Southern Hemisphere.

5.3 Biomass burning

Given the interannual variability in the mismatch, biomass burning is a prime candidate for being its driver. However, the mismatch between the modelled and measured time series at Darwin sees an overestimate of the X_{CO_2} by the model. This suggests that biomass burning is not the cause of this mismatch, as in general tropical biomass burning fluxes are likely to be underestimated, due to, for example, small fires not captured in satellite fire counts or those obscured by cloud (Randerson et al., 2012). In general, however, the good agreement between the timing of the measured X_{CO} and modelled biomass burning contribution to X_{CO_2} in Fig. 9, along with the absence of a signal at the time of the mismatch, suggests that any model–data disagreement due to

biomass burning is likely not caused by a mis-estimation of local biomass burning sources.

Figure 8 shows that biomass burning signals from remote regions are expected to manifest themselves in similar ways at each of the three sites. Therefore, any mismatch between measurements and models should be seen similarly at all three sites, but this is not the case – the mismatches are much smaller at Lauder, while the Wollongong time series does not overlap at the time of interest. The timing of the biomass burning signal at the sites (maximum at the change of the calendar year) would have the right phase to account for the Darwin anomaly, but the magnitude is far too small to account for the differences of up to 3 µmol mol^{-1} seen.

6 Conclusions

Through assessment of CO_2 tracers tagged by region and process, we have examined the drivers of variability in X_{CO_2} at the Southern Hemisphere TCCON sites. The local and remote terrestrial biosphere exert the dominant influence on changes in X_{CO_2}. At Darwin, these contribute seasonal variations of approximately 0.8 and 1.0 µmol mol^{-1}, respectively. At Lauder and Wollongong the remote terrestrial biosphere signals are of the order of 0.6 µmol mol^{-1}, while at Wollongong the Australian region also contributes a signal of a similar magnitude. In addition to the signals from the biosphere, local- and hemispheric-scale biomass burning can also provide signals above the limits of detectability to a total of approximately 0.4 µmol mol^{-1} on average. Comparison of model simulations with Southern Hemisphere TCCON measurements show that neither the CarbonTracker data assimilation system nor fluxes from the Simple Biosphere model capture the strong decrease in X_{CO_2} observed in the tropical monsoon season at Darwin, especially in 2006. This drawdown is associated with a monsoon season with an unusually early significant rainfall, which we propose results in early relief of water stress limits on photosynthesis. An extended time series of TCCON data and surface in situ trace gas measurements at Darwin will be crucial to confirming this hypothesis. The CarbonTracker model simulation shows better overall agreement with the data. However, both models show better agreement with each other than the measurements. The influence of interannual variability in dynamics is assessed, which contributes significantly in the monsoon period at Darwin, due to variation in ITCZ behaviour associated with the El Niño–Southern Oscillation. Overall, the Southern Hemisphere TCCON measurements provide additional information on CO_2 flux estimates in Australia, and the Southern Hemisphere would benefit from additional CO_2 measurements to constrain estimates of biospheric fluxes in this region.

Appendix A

A1 Instrumentation

All three sites are equipped with similar instrumentation: Bruker IFS125HR FTIR spectrometers. At Lauder a Bruker IFS120HR (the predecessor to the 125HR) was used from 2004 until 2010, when a 125HR instrument was commissioned and became the site's primary TCCON instrument. Spectra are simultaneously collected using two room-temperature operated detectors, indium gallium arsenide (InGaAs) covering 4000–11 000 cm^{-1} and silicon diode (Si) covering 10 000–30 000 cm^{-1}, with the spectral range restricted to below the laser frequency (15 798 cm^{-1}) by a red filter at 15 500 cm^{-1}.

To retrieve column amounts of the gases of interest, the program suite GGG described in Wunch et al. (2011b) is used. For this analysis we use the GGG version released on 24 February 2012, hereafter referred to as GGG2012. Carbon dioxide is retrieved from the spectra in two spectral windows, centred at 6220 and 6339.5 cm^{-1}. X_{CO_2} is calculated via ratioing to the retrieved oxygen column, retrieved in a window centred at 7885 cm^{-1}. Ratioing to the atmospheric O_2 column removes uncertainties and scatter caused by effects common to both the CO_2 and O_2 retrievals, such as surface pressure variations, which would mask flux signatures in the column abundances) and some instrumental errors, such as solar tracker pointing errors (Deutscher et al., 2010; Washenfelder et al., 2006; Wunch et al., 2011a). In addition, each site uses standard TCCON procedures, including the correction for source brightness fluctuations that also reduces scatter in the retrieved X_{CO_2} (Keppel-Aleks et al., 2007).

The spectral fitting is performed using a profile scaling technique. In this method, the shape of the vertical gas profile in the atmosphere is not changed, but is scaled iteratively to provide the best match between the measured spectrum, and that calculated from the derived gas amount, instrument function and spectroscopic parameters. The shape of the gas profile is set via the a priori – for CO_2 this is a daily profile based on a climatology generated from the GLOBALVIEW product (GLOBALVIEW-CO_2, 2011), changing with date and latitude. The stratospheric component of the profile is generated from the age of air relationship described by Andrews et al. (2001). The a priori profiles for each site and further details about them are given in Wunch et al. (2011b). A summary of the uncertainties associated with TCCON X_{CO_2} is also provided in Sect. 4b, Table 2 and Fig. 7 of the same publication. Prior to daily averaging, measurements are filtered based on a range of quality control criteria, including, but not limited to, solar zenith angles less than 82° and solar intensity variation of less than 5 % during the course of a scan.

A2 Data uncertainties

As a product of measurements, TCCON data are not without uncertainty. For example, despite the application of a correction for a known airmass-dependent artifact (Deutscher et al., 2010; Wunch et al., 2011b), some known airmass-dependent biases remain. To assess this effect, we vary the airmass corrections by ±50 % in a sensitivity study. This results in changes to the amplitude and phase of the seasonal cycle that depend on site. The maximum difference in the derived monthly means is ±0.2 μmol mol^{-1} at Wollongong, ±0.3 μmol mol^{-1} at Lauder, and smaller at Darwin due to the relatively smaller variation in air masses observed throughout the year. Other measurement uncertainties can occur due to instrument drifts and inter-site differences as well as the simple measurement repeatability. The instrument drifts and inter-site differences are minimized by detrending the time series and normalizing to a mean of 0 μmol mol^{-1}. The clear sky precision, a metric of measurement repeatability, has been estimated previously (Deutscher et al., 2010; Keppel-Aleks et al., 2007) from the standard deviation within a day as being better than 0.4 μmol mol^{-1}. Here, we are however interested in the ability of the measurement to capture the true average atmospheric state within a day or month, and we can therefore use the standard error to define its certainty. For daily means, and monthly means subsequently derived from the daily means, this is on average better than 0.1 μmol mol^{-1}. We combine this in quadrature with the uncertainty introduced by the airmass correction to yield an uncertainty of 0.32 μmol mol^{-1}. When looking at signals that might be detectable by these TCCON measurements, we therefore take a value larger than this, 0.4 μmol mol^{-1}, to constitute a detectable signal. This is a conservative estimate because it does not exploit any information about the phase of errors in the airmass correction.

A3 Comparing TCCON data to atmospheric models

When comparing the TCCON data to atmospheric model simulations, the a priori assumptions and vertical sensitivity of the retrieval need to be taken into account. This process, following the formulation of Rodgers and Connor (2003) is called smoothing, and requires knowledge of the TCCON a priori and averaging kernel. Wunch et al. (2010) recommended a slightly modified formulation because of the fact that the averaging kernels are calculated with respect to the retrieved, rather than the a priori, profile, however, the Wunch et al. (2010) and Rodgers and Connor (2003) formulations are negligibly different (< 0.1 μmol mol^{-1}). The smoothed X_{CO_2} values are described by the equation

$$c_s = c_a + h^T a^T (x_m - x_a), \quad \text{(A1)}$$

where c_s and c_a are the smoothed and a priori CO_2 columns, respectively, h describes the column summation, a is the FTS averaging kernel, in this case for CO_2 only, and x_m and x_a

are the model and a priori dry-air mole fractions. The averaging kernel describes the sensitivity of the retrieved column to changes in gas amounts at each of the retrieval grid levels. Variability in TCCON averaging kernels is largely dependent on the viewing geometry – i.e. the solar zenith angle. The solar zenith angle dependence of the averaging kernels is very similar between Southern Hemisphere sites, and indeed with those network-wide, as shown in Wunch et al. (2011b) for Lamont. We therefore use the standard site-independent TCCON averaging kernel product, which tabulates the averaging kernels at five degree solar zenith angle intervals. The standard product is interpolated to the measurement solar zenith angle to estimate the averaging kernel for the given measurement. We performed a sensitivity study to look at the effect of using the standard averaging kernel parameterization instead of the averaging kernels calculated for each retrieval, and the errors introduced are considerably smaller than 0.1 µmol mol^{-1}, even when extrapolating to low solar zenith angles at Darwin.

For each FTS measurement, we interpolate between the CT2011_oi model times that bracket the time of spectral collection, thereby generating a model profile corresponding to every measured CO_2 column. For comparison to the TCCON time series, we smooth the model output using the TCCON a priori and averaging kernels, following the formulation of Rodgers and Connor (2003). A smoothed model X_{CO_2} value is therefore created corresponding to each FTS X_{CO_2} measurement. In treating both the model and the measurement data in the same fashion we therefore eliminate potential biases in the comparison that could arise due to, for example, clear sky and daytime only sampling, as well as any bias that could occur from non-uniform time distribution of FTS measurements when averaging the FTS data to CT2011_oi time resolution. The difference in monthly means caused by the FTS sampling bias is calculated by comparing all daytime smoothed CT2011 X_{CO_2} values to those sampled at the FTS times, and the difference is less than 0.2 µmol mol^{-1}.

We have made no assessment of the accuracy of the stratospheric component of the model profiles, but any errors there could contribute to a spurious seasonal cycle.

The Supplement related to this article is available online at doi:10.5194/acp-14-9883-2014-supplement.

Acknowledgements. TCCON is funded by grant NNX11AG01G from NASA's Carbon Cycle Science Program. Measurements at Darwin are supported by Australian Research Council grant DP0879468 and NASA's Orbiting Carbon Observatory Project. The Lauder TCCON programme and TM3 model simulations are funded by NIWA under the New Zealand Greenhouse Gas Emissions, Mitigation, and Carbon Cycle Science Programme, and under the NZ Foundation of Research Science and Technology contracts C01X0204 and COX10406. CarbonTracker 2011_oi results provided by NOAA ESRL, Boulder, Colorado, USA from the website at http://carbontracker.noaa.gov. This work was also made possible by an RSNZ ISAT bilateral exchange grant and by grants from the Australian Research Council and Department of Innovation, Industry, Science and Research International Science Linkages project CG130014. Support for this work was also provided by the ESA GHG-CCI project. We gratefully acknowledge operational assistance from staff at the ARM site in Darwin. The authors acknowledge the constructive input of the two anonymous referees, whose feedback resulted in a much improved manuscript.

Edited by: T. Röckmann

References

Andreae, M. O. and Merlet, P.: Emission of trace gases and aerosols from biomass burning, Global Biogeochem. Cy., 15, 955–966, doi:10.1029/2000GB001382, 2001.

Andrews, A., Boering, K., Daube, B., Wofsy, S., Loewenstein, M., Jost, H., Podolske, J., Webster, C., Herman, R., Scott, D., Flesch, G., Moyer, E., Elkins, J., Dutton, G., Hurst, D., Moore, F., Ray, E., Romashkin, P., and Strahan, S.: Mean ages of stratospheric air derived from in situ observations of CO_2, CH_4, and N_2O, J. Geophys. Res., 106, 32295–32314, doi:10.1029/2001JD000465, 2001.

Baker, I., Denning, A., Hanan, N., Prihodko, L., Uliasz, M., Vidale, P., Davis, K., and Bakwin, P.: Simulated and observed fluxes of sensible and latent heat and CO_2 at the WLEF-TV tower using SiB2.5, Glob. Change Biol., 9, 1262–1277, doi:10.1046/j.1365-2486.2003.00671.x, 2003.

Basu, S., Houweling, S., Peters, W., Sweeney, C., Machida, T., Maksyutov, S., Patra, P. K., Saito, R., Chevallier, F., Niwa, Y., Matsueda, H., and Sawa, Y.: The seasonal cycle amplitude of total column CO_2: Factors behind the model-observation mismatch, J. Geophys. Res.-Atmos., 116, D23306, doi:10.1029/2011JD016124, 2011.

Bey, I., Jacob, D., Yantosca, R., Logan, J., Field, B., Fiore, A., Li, Q., Liu, H., Mickley, L., and Schultz, M.: Global modeling of tropospheric chemistry with assimilated meteorology: Model description and evaluation, J. Geophys. Res.-Atmos., 106, 23073–23095, doi:10.1029/2001JD000807, 2001.

Bovensmann, H., Buchwitz, M., Burrows, J. P., Reuter, M., Krings, T., Gerilowski, K., Schneising, O., Heymann, J., Tretner, A., and Erzinger, J.: A remote sensing technique for global monitoring of power plant CO_2 emissions from space and related applications, Atmos. Meas. Tech., 3, 781–811, doi:10.5194/amt-3-781-2010, 2010.

Burrows, J., Holzle, E., Goede, A., Visser, H., and Fricke, W.: SCIAMACHY - Scanning Imaging Absorption Spectrometer For Atmospheric Chartography, Acta Astronaut., 35, 445–451, doi:10.1016/0094-5765(94)00278-T, 1995.

Butz, A., Guerlet, S., Hasekamp, O., Schepers, D., Galli, A., Aben, I., Frankenberg, C., Hartmann, J.-M., Tran, H., Kuze, A., Keppel-Aleks, G., Toon, G., Wunch, D., Wennberg, P., Deutscher, N., Griffith, D., Macatangay, R., Messerschmidt, J., Notholt, J., and Warneke, T.: Toward accurate CO_2 and CH4 observations from GOSAT, Geophys. Res. Lett., 38, L14812, doi:10.1029/2011GL047888, 2011.

Chaves, M., Pereira, J., Maroco, J., Rodrigues, M., Ricardo, C., Osorio, M., Carvalho, I., Faria, T., and Pinheiro, C.: How plants cope with water stress in the field. Photosynthesis and growth, Ann. Bot., 89, 907–916, doi:10.1093/aob/mcf105, 2002.

Crisp, D., Atlas, R. M., Breon, F. M., Brown, L. R., Burrows, J. P., Ciais, P., Connor, B. J., Doney, S. C., Fung, I. Y., Jacob, D. J., Miller, C. E., O'Brien, D., Pawson, S., Randerson, J. T., Rayner, P., Salawitch, R. J., Sander, S. P., Sen, B., Stephens, G. L., Tans, P. P., Toon, G. C., Wennberg, P. O., Wofsy, S. C., Yung, Y. L., Kuang, Z., Chudasama, B., Sprague, G., Weiss, B., Pollock, R., Kenyon, D., and Schroll, S.: The Orbiting Carbon Observatory (OCO) mission, Adv. Space Res., 34, 700–709, 2004.

Crisp, D., Fisher, B. M., O'Dell, C., Frankenberg, C., Basilio, R., Bösch, H., Brown, L. R., Castano, R., Connor, B., Deutscher, N. M., Eldering, A., Griffith, D., Gunson, M., Kuze, A., Mandrake, L., McDuffie, J., Messerschmidt, J., Miller, C. E., Morino, I., Natraj, V., Notholt, J., O'Brien, D. M., Oyafuso, F., Polonsky, I., Robinson, J., Salawitch, R., Sherlock, V., Smyth, M., Suto, H., Taylor, T. E., Thompson, D. R., Wennberg, P. O., Wunch, D., and Yung, Y. L.: The ACOS CO_2 retrieval algorithm – Part II: Global X_{CO_2} data characterization, Atmos. Meas. Tech., 5, 687–707, doi:10.5194/amt-5-687-2012, 2012.

Denning, A., Collatz, G., Zhang, C., Randall, D., Berry, J., Sellers, P., Colello, G., and Dazlich, D.: Simulations of terrestrial carbon metabolism and atmospheric CO_2 in a general circulation model .1. Surface carbon fluxes, Tellus B, 48, 521–542, doi:10.1034/j.1600-0889.1996.t01-2-00009.x, 1996.

Denning, A. S., Holzer, M., Gurney, K. R., Heimann, M., Law, R. M., Rayner, P. J., Fung, I. Y., Fan, S.-M., Taguchi, S., Friedlingstein, P., Balkanski, Y., Taylor, J., Maiss, M., and Levin, I.: Three-dimensional transport and concentration of SF6, Tellus B, 51, 266–297, doi:10.1034/j.1600-0889.1999.00012.x, 1999.

Deutscher, N. M., Griffith, D. W. T., Bryant, G. W., Wennberg, P. O., Toon, G. C., Washenfelder, R. A., Keppel-Aleks, G., Wunch, D., Yavin, Y., Allen, N. T., Blavier, J.-F., Jiménez, R., Daube, B. C., Bright, A. V., Matross, D. M., Wofsy, S. C., and Park, S.: Total column CO_2 measurements at Darwin, Australia – site description and calibration against in situ aircraft profiles, Atmos. Meas. Tech., 3, 947–958, doi:10.5194/amt-3-947-2010, 2010.

Enting, I. G. and Mansbridge, J. V.: Seasonal sources and sinks of atmospheric CO_2 Direct inversion of filtered data, Tellus B, 41, 111–126, doi:10.1111/j.1600-0889.1989.tb00129.x, 1989.

GLOBALVIEW-CO_2: GLOBALVIEW-CO_2: Cooperative Atmospheric Data Integration Project – Carbon Dioxide., CD-ROM,

[Also available on Internet via anonymous FTP to ftp.cmdl.noaa.gov, Path: ccg/co2/GLOBALVIEW], 2011.

Griffith, D. W. T., Deutscher, N. M., Caldow, C., Kettlewell, G., Riggenbach, M., and Hammer, S.: A Fourier transform infrared trace gas and isotope analyser for atmospheric applications, Atmos. Meas. Techn., 5, 2481–2498, doi:10.5194/amt-5-2481-2012, 2012.

Gurney, K. R., Law, R. M., Denning, A. S., Rayner, P. J., Baker, D., Bousquet, P., Bruhwiler, L., Chen, Y.-H., Ciais, P., Fan, S., Fung, I. Y., Gloor, M., Heimann, M., Higuchi, K., John, J., Maki, T., Maksyutov, S., Masarie, K., Peylin, P., Prather, M., Pak, B. C., Randerson, J., Sarmiento, J., Taguchi, S., Takahashi, T., and Yuen, C.-W.: Towards robust regional estimates of CO_2 sources and sinks using atmospheric transport models, Nature, 415, 626–630, doi:10.1038/415626a, 2002.

Heimann, M. and Körner, S.: The global atmospheric tracer model TM3, Tech. Rep. 5, Max-Planck-Institut fuer Biogeochemie, Jena, Germany, 2003.

Houweling, S., Aben, I., Breon, F.-M., Chevallier, F., Deutscher, N., Engelen, R., Gerbig, C., Griffith, D., Hungershoefer, K., Macatangay, R., Marshall, J., Notholt, J., Peters, W., and Serrar, S.: The importance of transport model uncertainties for the estimation of CO_2 sources and sinks using satellite measurements, Atmos. Chem. Phys., 10, 9981–9992, doi:10.5194/acp-10-9981-2010, 2010.

Hurst, D., Griffith, D., Carras, J., Williams, D., and Fraser, P.: Measurements Of Trace Gases Emitted By Australian Savanna Fires During The 1990 Dry Season, J. Atmos. Chem., 18, 33–56, doi:10.1007/BF00694373, 1994.

Jacobson, A. R., Mikaloff Fletcher, S. E., Gruber, N., Sarmiento, J. L., and Gloor, M.: A joint atmosphere-ocean inversion for surface fluxes of carbon dioxide: 1. Methods and global-scale fluxes, Global Biogeochem. Cy., 21, GB1019, doi:10.1029/2005GB002556, 2007.

Jones, N., Rinsland, C., Liley, J., and Rosen, J.: Correlation of aerosol and carbon monoxide at 45 degrees S: Evidence of biomass burning emissions, Geophys. Res. Lett., 28, 709–712, doi:10.1029/2000GL012203, 2001.

Kalnay, E., Kanamitsu, M., Kistler, R., Collins, W., Deaven, D., Gandin, L., Iredell, M., Saha, S., White, G., Woollen, J., Zhu, Y., Leetmaa, A., Reynolds, R., Chelliah, M., Ebisuzaki, W., Higgins, W., Janowiak, J., Mo, K. C., Ropelewski, C., Wang, J., Jenne, R., and Joseph, D.: The NCEP/NCAR 40-Year Reanalysis Project, B. Am. Meteor. Soc., 77, 437–471, doi:10.1175/1520-0477(1996)077<0437:TNYRP>2.0.CO;2, 1996.

Keppel-Aleks, G., Toon, G. C., Wennberg, P. O., and Deutscher, N. M.: Reducing the impact of source brightness fluctuations on spectra obtained by Fourier-transform spectrometry, Appl. Opt., 46, 4774–4779, 2007.

Keppel-Aleks, G., Wennberg, P. O., and Schneider, T.: Sources of variations in total column carbon dioxide, Atmos. Chem. Phys., 11, 3581–3593, doi:10.5194/acp-11-3581-2011, 2011.

Keppel-Aleks, G., Wennberg, P. O., Washenfelder, R. A., Wunch, D., Schneider, T., Toon, G. C., Andres, R. J., Blavier, J.-F., Connor, B., Davis, K. J., Desai, A. R., Messerschmidt, J., Notholt, J., Roehl, C. M., Sherlock, V., Stephens, B. B., Vay, S. A., and Wofsy, S. C.: The imprint of surface fluxes and transport on variations in total column carbon dioxide, Biogeosciences, 9, 875–891, doi:10.5194/bg-9-875-2012, 2012.

Krol, M., Houweling, S., Bregman, B., van den Broek, M., Segers, A., van Velthoven, P., Peters, W., Dentener, F., and Bergamaschi, P.: The two-way nested global chemistry-transport zoom model TM5: algorithm and applications, Atmos. Chem. Phys., 5, 417–432, doi:10.5194/acp-5-417-2005, 2005.

Kuze, A., Suto, H., Nakajima, M., and Hamazaki, T.: Thermal and near infrared sensor for carbon observation Fourier-transform spectrometer on the Greenhouse Gases Observing Satellite for greenhouse gases monitoring, Appl. Opt., 48, 6716–6733, 2009.

Messerschmidt, J., Parazoo, N., Wunch, D., Deutscher, N. M., Roehl, C., Warneke, T., and Wennberg, P. O.: Evaluation of seasonal atmosphere–biosphere exchange estimations with TCCON measurements, Atmos. Chem. Phys., 13, 5103–5115, doi:10.5194/acp-13-5103-2013, 2013.

Morino, I., Uchino, O., Inoue, M., Yoshida, Y., Yokota, T., Wennberg, P. O., Toon, G. C., Wunch, D., Roehl, C. M., Notholt, J., Warneke, T., Messerschmidt, J., Griffith, D. W. T., Deutscher, N. M., Sherlock, V., Connor, B., Robinson, J., Sussmann, R., and Rettinger, M.: Preliminary validation of column-averaged volume mixing ratios of carbon dioxide and methane retrieved from GOSAT short-wavelength infrared spectra, Atmos. Meas. Tech., 4, 1061–1076, doi:10.5194/amt-4-1061-2011, 2011.

Mu, M., Randerson, J. T., van der Werf, G. R., Giglio, L., Kasibhatla, P., Morton, D., Collatz, G. J., DeFries, R. S., Hyer, E. J., Prins, E. M., Griffith, D. W. T., Wunch, D., Toon, G. C., Sherlock, V., and Wennberg, P. O.: Daily and 3-hourly variability in global fire emissions and consequences for atmospheric model predictions of carbon monoxide, J. Geophys. Res.-Atmos., 116, D24303, doi:10.1029/2011JD016245, 2011.

Nara, H., Tanimoto, H., Nojiri, Y., Mukai, H., Zeng, J., Tohjima, Y., and Machida, T.: CO emissions from biomass burning in South-east Asia in the 2006 El Nino year: shipboard and AIRS satellite observations, Environ. Chem., 8, 213–223, doi:10.1071/EN10113, 2011.

Nevison, C. D., Mahowald, N. M., Doney, S. C., Lima, I. D., van der Werf, G. R., Randerson, J. T., Baker, D. F., Kasibhatla, P., and McKinley, G. A.: Contribution of ocean, fossil fuel, land biosphere, and biomass burning carbon fluxes to seasonal and interannual variability in atmospheric CO_2, J. Geophys. Res.-Biogeo., 113, G01010, doi:10.1029/2007JG000408, 2008.

Niwa, Y., Machida, T., Sawa, Y., Matsueda, H., Schuck, T. J., Brenninkmeijer, C. A. M., Imasu, R., and Satoh, M.: Imposing strong constraints on tropical terrestrial CO_2 fluxes using passenger aircraft based measurements, J. Geophys. Res.-Atmos., 117, D11303, doi:10.1029/2012JD017474, 2012.

Oda, T. and Maksyutov, S.: A very high-resolution (1 km $\times$ 1 km) global fossil fuel CO_2 emission inventory derived using a point source database and satellite observations of nighttime lights, Atmos. Chem. Phys., 11, 543–556, doi:10.5194/acp-11-543-2011, 2011.

Paton-Walsh, C., Deutscher, N. M., Griffith, D. W. T., Forgan, B. W., Wilson, S. R., Jones, N. B., and Edwards, D. P.: Trace gas emissions from savanna fires in northern Australia, J. Geophys. Res., 115, D16314, doi:10.1029/2009JD013309, 2010.

Peters, W., Krol, M. C., Dlugokencky, E. J., Dentener, F. J., Bergamaschi, P., Dutton, G., Velthoven, P. v., Miller, J. B., Bruhwiler, L., and Tans, P. P.: Toward regional-scale modeling using the two-way nested global model TM5: Characterization of

transport using SF6, J. Geophys. Res.-Atmos., 109, D19314, doi:10.1029/2004JD005020, 2004.

Peters, W., Jacobson, A. R., Sweeney, C., Andrews, A. E., Conway, T. J., Masarie, K., Miller, J. B., Bruhwiler, L. M. P., Pétron, G., Hirsch, A. I., Worthy, D. E. J., van der Werf, G. R., Randerson, J. T., Wennberg, P. O., Krol, M. C., and Tans, P. P.: An atmospheric perspective on North American carbon dioxide exchange: CarbonTracker, P. Natl. Acad. Sci., 104, 18925–18930, doi:10.1073/pnas.0708986104, 2007.

Peylin, P., Law, R. M., Gurney, K. R., Chevallier, F., Jacobson, A. R., Maki, T., Niwa, Y., Patra, P. K., Peters, W., Rayner, P. J., Rödenbeck, C., van der Laan-Luijkx, I. T., and Zhang, X.: Global atmospheric carbon budget: results from an ensemble of atmospheric CO_2 inversions, Biogeosciences, 10, 6699–6720, doi:10.5194/bg-10-6699-2013, 2013.

Poulter, B., Frank, D., Ciais, P., Myneni, R. B., Andela, N., Bi, J., Broquet, G., Canadell, J. G., Chevallier, F., Liu, Y. Y., Running, S. W., Sitch, S., and van der Werf, G. R.: Contribution of semi-arid ecosystems to interannual variability of the global carbon cycle, Nature, 509, 600–603, doi:10.1038/nature13376, 2014.

Randerson, J. T., Chen, Y., van der Werf, G. R., Rogers, B. M., and Morton, D. C.: Global burned area and biomass burning emissions from small fires, J. Geophys. Res.-Biogeo., 117, G04012, doi:10.1029/2012JG002128, 2012.

Reuter, M., Bovensmann, H., Buchwitz, M., Burrows, J. P., Connor, B. J., Deutscher, N. M., Griffith, D. W. T., Heymann, J., Keppel-Aleks, G., Messerschmidt, J., Notholt, J., Petri, C., Robinson, J., Schneising, O., Sherlock, V., Velazco, V., Warneke, T., Wennberg, P. O., and Wunch, D.: Retrieval of atmospheric CO_2 with enhanced accuracy and precision from SCIAMACHY: Validation with FTS measurements and comparison with model results, J. Geophys. Res., 116, D04301, doi:10.1029/2010JD015047, 2011.

Rodgers, C. D. and Connor, B. J.: Intercomparison of remote sounding instruments, J. Geophys. Res., 108, 4116, doi:10.1029/2002JD002299, 2003.

Sellers, P., Mintz, Y., Sud, Y., and Dalcher, A.: A Simple Biosphere Model (SIB) For Use Within General-circulation Models, J. Atmos. Sci., 43, 505–531, doi:10.1175/1520-0469(1986)043<0505:ASBMFU>2.0.CO;2, 1986.

Stephens, B. B., Gurney, K. R., Tans, P. P., Sweeney, C., Peters, W., Bruhwiler, L., Ciais, P., Ramonet, M., Bousquet, P., Nakazawa, T., Aoki, S., Machida, T., Inoue, G., Vinnichenko, N., Lloyd, J., Jordan, A., Heimann, M., Shibistova, O., Langenfelds, R. L., Steele, L. P., Francey, R. J., and Denning, A. S.: Weak Northern and Strong Tropical Land Carbon Uptake from Vertical Profiles of Atmospheric CO_2, Science, 316, 1732–1735, doi:10.1126/science.1137004, 2007.

Tans, P., Fung, I., and Takahashi, T.: Observational Constraints On The Global Atmospheric CO_2 Budget, Science, 247, 1431–1438, doi:10.1126/science.247.4949.1431, 1990.

Valsala, V., Tiwari, Y. K., Pillai, P., Roxy, M., Maksyutov, S., and Murtugudde, R.: Intraseasonal variability of terrestrial biospheric CO_2 fluxes over India during summer monsoons, J. Geophys. Res.-Biogeo., 118, 752–769, doi:10.1002/jgrg.20037, 2013.

van der Werf, G. R., Randerson, J. T., Giglio, L., Collatz, G. J., Mu, M., Kasibhatla, P. S., Morton, D. C., DeFries, R. S., Jin, Y., and van Leeuwen, T. T.: Global fire emissions and the contribution of deforestation, savanna, forest, agricultural, and peat fires (1997–2009), Atmos. Chem. Phys., 10, 11707–11735, doi:10.5194/acp-10-11707-2010, 2010.

Washenfelder, R. A., Toon, G. C., Blavier, J.-F., Yang, Z., Allen, N. T., Wennberg, P. O., Vay, S. A., Matross, D. M., and Daube, B. C.: Carbon dioxide column abundances at the Wisconsin Tall Tower site, J. Geophys. Res., 111, D22305, doi:10.1029/2006JD007154, 2006.

Wofsy, S. C., Team, H. S., Team, C. M., and Team, S.: HIAPER Pole-to-Pole Observations (HIPPO): fine-grained, global-scale measurements of climatically important atmospheric gases and aerosols, Philos. T. R. Soc. A, 369, 2073–2086, doi:10.1098/rsta.2010.0313, 2011.

Wunch, D., Toon, G. C., Wennberg, P. O., Wofsy, S. C., Stephens, B. B., Fischer, M. L., Uchino, O., Abshire, J. B., Bernath, P., Biraud, S. C., Blavier, J.-F. L., Boone, C., Bowman, K. P., Browell, E. V., Campos, T., Connor, B. J., Daube, B. C., Deutscher, N. M., Diao, M., Elkins, J. W., Gerbig, C., Gottlieb, E., Griffith, D. W. T., Hurst, D. F., Jiménez, R., Keppel-Aleks, G., Kort, E. A., Macatangay, R., Machida, T., Matsueda, H., Moore, F., Morino, I., Park, S., Robinson, J., Roehl, C. M., Sawa, Y., Sherlock, V., Sweeney, C., Tanaka, T., and Zondlo, M. A.: Calibration of the Total Carbon Column Observing Network using aircraft profile data, Atmos. Meas. Tech., 3, 1351–1362, doi:10.5194/amt-3-1351-2010, 2010.

Wunch, D., Toon, G. C., Blavier, J. F. L., Washenfelder, R. A., Notholt, J., Connor, B. J., Griffith, D. W. T., Sherlock, V., and Wennberg, P. O.: The Total Carbon Column Observing Network, Philos. T. R. Soc. A, 369, 2087–2112, doi:10.1098/rsta.2010.0240, 2011a.

Wunch, D., Wennberg, P. O., Toon, G. C., Connor, B. J., Fisher, B., Osterman, G. B., Frankenberg, C., Mandrake, L., O'Dell, C., Ahonen, P., Biraud, S. C., Castano, R., Cressie, N., Crisp, D., Deutscher, N. M., Eldering, A., Fisher, M. L., Griffith, D. W. T., Gunson, M., Heikkinen, P., Keppel-Aleks, G., Kyrö, E., Lindenmaier, R., Macatangay, R., Mendonca, J., Messerschmidt, J., Miller, C. E., Morino, I., Notholt, J., Oyafuso, F. A., Rettinger, M., Robinson, J., Roehl, C. M., Salawitch, R. J., Sherlock, V., Strong, K., Sussmann, R., Tanaka, T., Thompson, D. R., Uchino, O., Warneke, T., and Wofsy, S. C.: A method for evaluating bias in global measurements of CO_2 total columns from space, Atmos. Chem. Phys., 11, 12317–12337, doi:10.5194/acp-11-12317-2011, 2011b.

Yang, Z., Washenfelder, R. A., Keppel-Aleks, G., Krakauer, N. Y., Randerson, J. T., Tans, P. P., Sweeney, C., and Wennberg, P. O.: New constraints on Northern Hemisphere growing season net flux, Geophys. Res. Lett., 34, L12807, doi:10.1029/2007GL029742, 2007.

Zhang, J., Smith, K. R., Ma, Y., Ye, S., Jiang, F., Qi, W., Liu, P., Khalil, M. A. K., Rasmussen, R. A., and Thorneloe, S. A.: Greenhouse gases and other airborne pollutants from household stoves in China: a database for emission factors, Atmos. Environ., 34, 4537–4549, doi:10.1016/S1352-2310(99)00450-1, 2000.